Sensing Analysis of Piezoelectric Composite Beam

EVA KORMANIKOVA, KAMILA KOTRASOVA
Institute of Structural Engineering,
Civil Engineering Faculty, Technical University of Kosice,
Vysokoskolska 4, 04200 Kosice,
SLOVAKIA

Abstract: - The objective of this paper is to analyze the smart composite beam integrated with a piezoelectric layer to use in sensing simulation. The beam consists of an 8-layered $[0/45/-45/90]_S$ bottom CFRP composite layer and an upper PZT layer as a piezoelectric sensor. Linear 3D piezo-elasticity theory for static analysis has been utilized. A prescribed downward displacement is applied at the free end of the cantilever beam to obtain the voltage and electric field results of the outer surface of the piezoelectric layer. The analysis of the piezoelectric composite beam is performed by ADINA FEM analysis.

Key-Words: - Sensing static analysis, FEM, 3D modeling, piezoelectricity, composite, cantilever beam.

Received: July 11, 2023. Revised: March 4, 2024. Accepted: May 11, 2024. Published: June 26, 2024.

1 Introduction

Piezoelectric materials exhibit certain special characteristics that make them important engineering materials. The materials belong to the class of smart materials because they exhibit inherent transducer characteristics. The discovery of ferroelectric ceramics barium titanate, and lead zirconate titanate (PZT) during the 1940s and 1950s led to a spate of research activities on these materials. Over the years, a wide variety of transducers, sensors, and actuators have been developed using the ceramic PZT, which is one of the most sensitive piezoelectric materials. Another important piezoelectric material that has created a lot of interest is the polymer polyvinylidene fluoride (PVDF), which was discovered in 1969. A polymer exhibiting transducer characteristics has special advantages over ceramic because of the more flexible and less brittle nature of polymers. Zinc oxide is a relatively newfound piezoelectric material that has been used in nano-crystalline form for piezoelectric applications such as micro-actuators and sensing devices, [1], [2]. Piezoelectric sensors and actuators are widely used in smart systems, [3], [4], [5].

2 Problem Formulation

When a dielectric material belonging to a noncentrosymmetric class (except the octahedral class) is subjected to an external electric eld, there will be asymmetric movement of the neighboring ions, resulting in significant deformation of the crystal and the deformation is directly proportional to the applied electric eld. These materials exhibit an electrostrictive effect due to the anharmonicity of the bonds, but it is masked by the more significant asymmetric displacement. The materials are called piezoelectric materials. Piezoelectric materials exhibit certain special characteristics that make them important engineering materials. The materials belong to the class of smart materials because they exhibit inherent transducer characteristics, [6], [7], [8].

2.1 Constitutive Equation

A piezoelectric material that is exposed to the small electric field and low levels of mechanical stress exhibits characteristics of linear behavior, [1]. The constitutive equations describing the linear behavior of the piezoelectric material are based on the assumption that the resulting deformation is composed of the deformation caused by the mechanical stress and the deformation caused by the electric voltage applied to the electrodes of the piezoelectric material.

2.1.1 Expression using σ and E

Using the symmetrical properties of tensor quantities, we can express the constitutive equations using the tensor of mechanical stress **σ** and vector of electric field intensity **E** as [6]

$$D_i = \epsilon_{ik}^{\sigma} E_k + d_{iq}\sigma_q \quad (1)$$

$$\varepsilon_p = d_{pk}E_k + s_{pq}^{E}\sigma_q \quad (2)$$

2.1.2 Expression using ϵ and E

The second variant of the constitutive law is expressed using the overall deformation field **ϵ** and intensity of the electric field **E** as

$$\sigma_p = c_{pq}^E \varepsilon_p - e_{pk} E_k \tag{3}$$

$$D_i = e_{iq} \varepsilon_q + \epsilon_{ik}^{\varepsilon} E_k \tag{4}$$

where:

D_i and E_k are the components of the vector of electric induction (electric displacement field) and electric intensity, respectively.

ϵ_{ik}^{σ} - permittivity at constant stress

$\epsilon_{ik}^{\varepsilon}$ - permittivity at constant strain

σ_q - coefficients of the stress vector

ε_p - coefficients of strain vector

s_{pq}^E - coefficients of the tensor of elasticity constants for the constant electrical field

d_{iq} , d_{pk}, e_{pk}, e_{iq} are piezoelectric coefficients.

For PZT material, that is polled in the *z*-direction, the equations (1), (2) are written in the form

$$\begin{pmatrix} D_1 \\ D_2 \\ D_2 \end{pmatrix} = \begin{pmatrix} \epsilon_{11}^{\sigma} & 0 & 0 \\ 0 & \epsilon_{22}^{\sigma} & 0 \\ 0 & 0 & \epsilon_{33}^{\sigma} \end{pmatrix} \begin{pmatrix} E_1 \\ E_2 \\ E_2 \end{pmatrix} + \\ + \begin{pmatrix} 0 & 0 & 0 & 0 & d_{15} & 0 \\ 0 & 0 & 0 & d_{15} & 0 & 0 \\ d_{31} & d_{33} & d_{33} & 0 & 0 & 0 \end{pmatrix} \begin{pmatrix} \sigma_1 \\ \sigma_2 \\ \sigma_3 \\ \sigma_4 \\ \sigma_5 \\ \sigma_6 \end{pmatrix} \tag{5}$$

$$\begin{pmatrix} \varepsilon_1 \\ \varepsilon_2 \\ \varepsilon_3 \\ \varepsilon_4 \\ \varepsilon_5 \\ \varepsilon_6 \end{pmatrix} = \begin{pmatrix} 0 & 0 & d_{31} \\ 0 & 0 & d_{31} \\ 0 & 0 & d_{33} \\ 0 & d_{15} & 0 \\ d_{15} & 0 & 0 \\ 0 & 0 & 0 \end{pmatrix} \begin{pmatrix} E_1 \\ E_2 \\ E_2 \end{pmatrix} + \\ \begin{pmatrix} s_{11}^E & s_{12}^E & s_{13}^E & 0 & 0 & 0 \\ s_{12}^E & s_{11}^E & s_{13}^E & 0 & 0 & 0 \\ s_{13}^E & s_{13}^E & s_{33}^E & 0 & 0 & 0 \\ 0 & 0 & 0 & s_{44}^E & 0 & 0 \\ 0 & 0 & 0 & 0 & s_{44}^E & 0 \\ 0 & 0 & 0 & 0 & 0 & 2s_{11}^E - s_{12}^E \end{pmatrix} \begin{pmatrix} \sigma_1 \\ \sigma_2 \\ \sigma_3 \\ \sigma_4 \\ \sigma_5 \\ \sigma_6 \end{pmatrix} \tag{6}$$

Constitutive equations (3-4) can be written in the form

$$\boldsymbol{\sigma} = \mathbf{c}^E \boldsymbol{\varepsilon} - \mathbf{e}^T \mathbf{E} \tag{7}$$

$$\mathbf{D} = \boldsymbol{e}\boldsymbol{\varepsilon} - \epsilon^{\varepsilon} \mathbf{E} \tag{8}$$

where

$$\boldsymbol{\varepsilon} = \begin{pmatrix} \varepsilon_x \\ \varepsilon_y \\ \varepsilon_z \\ \gamma_{yz} \\ \gamma_{xz} \\ \gamma_{xy} \end{pmatrix} = \begin{pmatrix} \partial u/\partial x \\ \partial v/\partial y \\ \partial w/\partial z \\ \partial v/\partial z + \partial w/\partial y \\ \partial v/\partial x + \partial u/\partial z \\ \partial v/\partial x + \partial u/\partial y \end{pmatrix} \tag{9}$$

3 Finite Element Method

In FE analysis, the piezoelectric medium is divided into several small discrete elements called finite elements. Each element has a set of interconnecting points on its edges called the nodes. The variables, called the degrees of freedom (DOF), such as displacement, potential, etc., at any arbitrary point within an element are expressed in terms of their values at the nodal points, using a suitable polynomial interpolation function N_i defined for each variable, [9], [10].

For an element with *n* nodes, the displacement of a point (*x*, *y*, *z*), denoted by $u(x,y,z)$, is expressed in terms of the nodal displacement values $u_i(x,y,z)$ by

$$u = \sum_{i=1}^{n} N_i u_i \tag{10}$$

$$v = \sum_{i=1}^{n} N_i v_i \tag{11}$$

$$w = \sum_{i=1}^{n} N_i w_i \tag{12}$$

Then for the strain vector can be written:

$$\boldsymbol{\varepsilon} = \begin{pmatrix} \varepsilon_x \\ \varepsilon_y \\ \varepsilon_z \\ \gamma_{yz} \\ \gamma_{xz} \\ \gamma_{xy} \end{pmatrix} = \begin{pmatrix} \partial \sum_{i=1}^{n} N_i u_i /\partial x \\ \partial \sum_{i=1}^{n} N_i v_i /\partial y \\ \partial \sum_{i=1}^{n} N_i w_i /\partial z \\ \partial \sum_{i=1}^{n} N_i v_i /\partial z + \partial \sum_{i=1}^{n} N_i w_i /\partial y \\ \partial \sum_{i=1}^{n} N_i w_i /\partial x + \partial \sum_{i=1}^{n} N_i u_i /\partial z \\ \partial \sum_{i=1}^{n} N_i v_i /\partial x + \partial \sum_{i=1}^{n} N_i u_i /\partial y \end{pmatrix} \tag{13}$$

with the simplest notation

$$\boldsymbol{\varepsilon} = \mathbf{B}_u \mathbf{u}^e \tag{14}$$

where matrix $\mathbf{B}_u$ contains submatrices $\mathbf{N}_x$, $\mathbf{N}_y$ and $\mathbf{N}_z$ that are derivations of shape function over *x*,*y*,*z*, respectively

$$\mathbf{B}_u = \begin{pmatrix} \mathbf{N}_x & 0 & 0 \\ 0 & \mathbf{N}_y & 0 \\ 0 & 0 & \mathbf{N}_z \\ 0 & \mathbf{N}_z & \mathbf{N}_y \\ \mathbf{N}_z & 0 & \mathbf{N}_x \\ \mathbf{N}_y & \mathbf{N}_x & 0 \end{pmatrix} \tag{15}$$

and

$$\mathbf{u}^e = (u_1 \dots u_n \;\; v_1 \dots v_n \;\; w_1 \dots w_n)^T \tag{16}$$

The electric field in terms of electric potential φ is given by

$$\mathbf{E} = -\boldsymbol{\nabla}\varphi \tag{17}$$

or in the form

$$\mathbf{E} = \begin{pmatrix} E_x \\ E_y \\ E_z \end{pmatrix} = -\begin{pmatrix} \partial\varphi/\partial x \\ \partial\varphi/\partial y \\ \partial\varphi/\partial z \end{pmatrix} \tag{18}$$

where φ is the electric potential.

The potential at the point (*x*,*y*,*z*), denoted by φ(*x*,*y*,*z*), is expressed in terms of the nodal potential values φ_i (*x*,*y*,*z*) by

$$\varphi = \sum_{i=1}^{n} N_i \varphi_i \tag{19}$$

and the Eq. 18 can be written

$$\mathbf{E} = -\begin{pmatrix} \frac{\partial \sum_{i=1}^{n} N_i \varphi_i}{\partial x} \\ \frac{\partial \sum_{i=1}^{n} N_i \varphi_i}{\partial y} \\ \frac{\partial \sum_{i=1}^{n} N_i \varphi_i}{\partial z} \end{pmatrix} = -\mathbf{B}_\varphi \boldsymbol{\varphi}^e \tag{20}$$

where matrix $\mathbf{B}_\varphi$ contains submatrices $\mathbf{N}_x$, $\mathbf{N}_y$ and $\mathbf{N}_z$ that are derivations of shape function over *x*,*y*,*z*, respectively

$$\mathbf{B}_\varphi = \begin{pmatrix} \mathbf{N}_x \\ \mathbf{N}_y \\ \mathbf{N}_z \end{pmatrix} \tag{21}$$

and

$$\boldsymbol{\varphi}^e = (\varphi_1 \dots \varphi_n)^T \tag{22}$$

For static analysis of virtual work of internal forces and virtual work of external mechanical forces can be written

$$\int_V \delta\boldsymbol{\varepsilon}^T \boldsymbol{\sigma} dV = \delta u^{eT} \mathbf{F}^e \tag{23}$$

where $\mathbf{F}^e$ represents vector of external nodal forces

$$\mathbf{F}^e = \left(F_{x1} \dots F_{xn} \;\; F_{y1} \dots F_{yn} \;\; F_{z1} \dots F_{zn}\right)^T \tag{24}$$

Similarly, for virtual internal work of the electric field and external work of electric charge can be written

$$-\int_V \delta\mathbf{E}^T \mathbf{D} dV = \delta\varphi^{eT} \mathbf{Q}^e \tag{25}$$

where $\mathbf{Q}^e$ represents vector of external nodal charges

$$\mathbf{Q}^e = (Q_1 \dots Q_n)^T$$

By substituting the Eqs. 13 and 20 into Eqs. 7 and 8 we can write constitutive equations in the form

$$\boldsymbol{\sigma} = \mathbf{c}^E \mathbf{B}_u \mathbf{u}^e + \mathbf{e}^T \mathbf{B}_\varphi \varphi^e \tag{26}$$

$$\mathbf{D} = \boldsymbol{e} \mathbf{B}_u \mathbf{u}^e - \epsilon^\epsilon \mathbf{B}_\varphi \varphi^e \tag{27}$$

For virtual strain and electric fields

$$\delta\boldsymbol{\varepsilon} = \mathbf{B}_u \delta\mathbf{u}^e \tag{28}$$

$$\delta\mathbf{E} = -\mathbf{B}_\varphi \delta\boldsymbol{\varphi}^e \tag{29}$$

By substituting the Eqs. 26 - 29 into Eqs. 23 and 25 we get

$$\begin{pmatrix} \mathbf{K}_{uu}^e & \mathbf{K}_{u\varphi}^e \\ \mathbf{K}_{\varphi u}^e & \mathbf{K}_{\varphi\varphi}^e \end{pmatrix} \begin{pmatrix} \mathbf{u}^e \\ \boldsymbol{\varphi}^e \end{pmatrix} = \begin{pmatrix} \mathbf{F}^e \\ \mathbf{Q}^e \end{pmatrix} \tag{30}$$

where individual submatrices have the form

$$\mathbf{K}_{uu}^e = \int_V \boldsymbol{B}_u^T \boldsymbol{c}^E \mathbf{B}_u dV \tag{31}$$

$$\mathbf{K}_{u\varphi}^e = \int_V \boldsymbol{B}_u^T \boldsymbol{e}^T \mathbf{B}_\varphi dV \tag{32}$$

$$\mathbf{K}_{\varphi u}^e = \int_V \boldsymbol{B}_\varphi^T \boldsymbol{e} \mathbf{B}_u dV \tag{33}$$

$$\mathbf{K}_{\varphi\varphi}^e = -\int_V \boldsymbol{B}_\varphi^T \epsilon^\varepsilon \mathbf{B}_\varphi dV \tag{34}$$

Solving Eq.30 yields the value of the displacement *u* and the electrical potential *φ* at various points in the piezoelectric medium. Using the *u* and *φ* values, the strain and the electric field in the medium can be computed from Eqs. 14 and 20.

4 Problem Solution

This paper deals with piezoelectric unimorph. The piezoelectric unimorph is a cantilever beam consisting of a single strip of piezoelectric material clamped at one end and free at the other end (Figure 1). The bending of the cantilever on the application of displacement is used for sensing analysis. The unimorph is made of a thin film of piezoelectric material formed on a non-piezoelectric substrate material. The system is clamped at one end, and a displacement is applied at the free end, and we investigate the voltage and electric field results. The unimorph is used in d_{33} mode (Figure 1). In d_{31} mode, the piezoelectric layer is poled in a direction perpendicular to the plane (direction 3) as shown in Figure 1. Due to the transverse piezoelectric effect, the piezoelectric film expands in the transverse direction, which is direction 1. This results in the bending of the unimorph. Using microelectromechanical systems (MEMS) micromachining techniques, micron-size piezoelectric unimorph sensors have been fabricated. The piezoelectric films are deposited on silicon oxide or silicon nitride substrates. The piezoelectric material used is PZT. The surface micromachining technique is used for the fabrication of the cantilever structure.

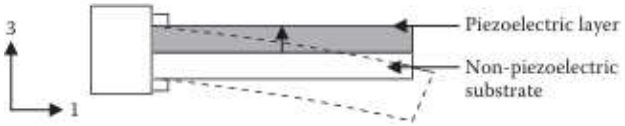

Fig. 1: Piezoelectric unimorph cantilever beam in d_{33} mode: the piezoelectric layer is poled in direction 3, and the material is strained in the same direction

The cantilever shown below in Figure 2 is composed of two sublayers: the top sublayer is a piezoelectric material, and the bottom sublayer is an elastic CFRP material. The interface between the two layers is grounded. The 3-D FE analysis of an unimorph cantilever is described.

The dimensions of the cantilever are (Figure 2): L = 0.1m, W = 0.01m, h_1= 0.001m, h_2 =0.004m. The material properties of the bottom sublayer made of 8-layered $[0/45/-45/90]_S$ CFRP composite are: E_1 = 140 GPa, $E_2 = E_3$ = 12.3 GPa, $G_{12} = G_{13} = G_{23}$ = 6.5 GPa, $\nu_{12} = \nu_{13} = \nu_{23}$ = 0.38. After homogenization, [11], [12] of the sublayer: E = 56,352 GPa, ν_{23} = 0.315.

The piezoelectric material properties are:

Elastic constants: $E_1 = E_2$ = 61 GPa, E_3 = 53.2 GPa, ν_{12} = 0.35, $\nu_{13} = \nu_{23}$ = 0.38, G_{12} = 22.593 GPa, $G_{13} = G_{23}$ = 21.1 GPa.

Coupling constants: $e_{13} = e_{23}$ = − 7.209 N/Vm, e_{33} = 15.118 N/Vm, $e_{51} = e_{62}$ = 12.332 N/Vm (where 1=x, 2=y, 3=z, 4=xy, 5=xz, 6=yz)

Dielectric constants: $\varepsilon_{11} = \varepsilon_{22}$ = 1.53x10^{-8} C/Vm, ε_{33} = 1.5x10^{-8} C/Vm.

The polarization (P) of the piezoelectric material is along the z-direction (Figure 2). All the nodes on the grounded face are made to have zero potential. A prescribed downward displacement of 0.005 m is applied at the free end of the cantilever beam.

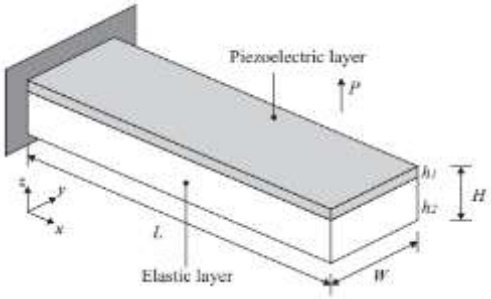

Fig. 2: Dimensions of the cantilever beam

The way of modeling the example is following:

Model definition by 3D solid element with piezoelectric option,

Defining the piezoelectric material polarization direction,

Defining the piezoelectric element group is a mesh generation of elements in an element group,

Defining the material axis as the same with global axes direction,

Defining the structural and piezoelectric boundary conditions and loading in the form of displacement,

Plotting voltage and electric field results.

In Figure 3 can be seen the original and deformed cantilever beam under displacement loading and cutting line 'MIDLINE' for the variation of the electric field z along the line in meshing form.

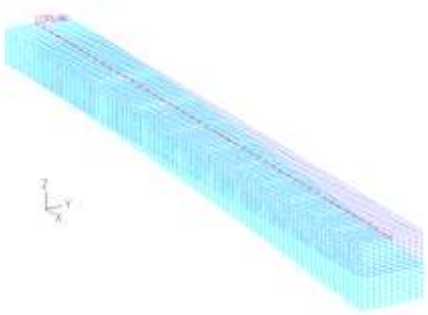

Fig. 3: Original and deformed cantilever beam under displacement loading

In Figure 4 can be seen the variation of the electric field *z* along the line 'MIDLINE' through the length of the beam. The maximum value of electric field *z* is $2.20652.10^6$ V/m at a distance of 2.08333 mm.

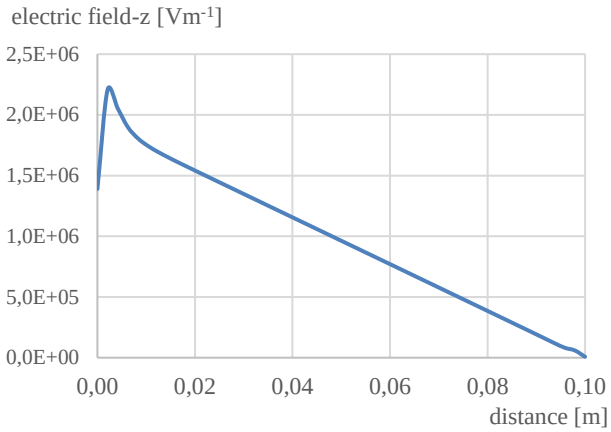

Fig. 4: Electric field z along the middle line of a cantilever beam

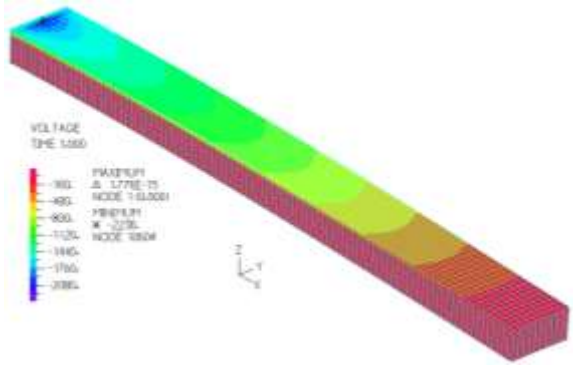

Fig. 5: Voltage along the beam length

We used the loading in the form of displacement and performed the sensing analysis. Material properties of interest in the analysis of piezoelectric materials are: i. Components of the piezoelectric coefficient matrix, ii. Components of dielectric constant matrix, iii. Components of elastic stiffness or compliance constant matrix. The homogenization of an 8-layered $[0/45/-45/90]_S$ CFRP composite is done to obtain the effective elastic properties. The piezoelectric medium requires both mechanical and electrical constraints to be specified: i. Mechanical constraints: The mechanical DOF displacement components of all the nodes on the clamped parts of the structure are made zero. ii. Electrical constraints: The electrical DOF potential on all the nodes on the electrode faces of the piezoelectric material that need to be earthed are made zero.

5 Conclusion

The linear 3D piezo-elasticity theory for static ADINA FEM analysis of the piezoelectric composite beam has been utilized for obtaining the voltage and electric field *z* under vertical displacement 0.005 m. The maximum value of electric field *z* is $2.20652.10^6$ V/m at a distance of 2.08333 mm (Figure 4). The maximum voltage -2238 V (Figure 5) is at the clamped end of the unimorph.

By changing the dimensions of the unimorph and the clamping conditions, higher voltage can be achieved at lower displacement, [13], [14], [15], [16]. It would be interesting to apply the choice of the numerical mesh size for instance by reporting a convergence analysis on the number of elements and the error analysis of the numerical method, that we will investigate in the further research study.

Acknowledgments:
We thank the Scientific Grant Agency of the Ministry of Education of the Slovak Republic and the Slovak Academy of Sciences under Projects VEGA1/0363/21, and VEGA 1/0307/23.

References:

[1] M. S. Vijaya, *Piezoelectric Materials and Devices*, CRC Press, Taylor & Francis Group, 2013.

[2] G. Park, H. H. Cudney, D. J. Inman, Impedance-based health monitoring of civil structural components, *Journal of Infrastructure Systems* 6(4) (2000), pp. 153–160, https://doi.org/10.1061/(ASCE)1076-0342(2000)6:4(153).

[3] L. Kormanikova, E. Kormanikova, D. Katunsky, Shape Design and Analysis of Adaptive Structures, *Procedia Engineering* 190 2017, pp. 7-14, http://dx.doi.org/10.1016/j.proeng.2017.05.300.

[4] L. Kabosova, I. Foged, S. Kmet, D. Katunsky, Hybrid design method for wind-adaptive architecture, *International Journal of Architectural Computing* 17(4) 2019, pp. 307-322, http://dx.doi.org/10.1177/1478077119886528.

[5] D. Magliacano, M. Viscardi, I. Dimino, A. Concilio, Active vibration control by piezoceramic actuators of a car floor panel, *ICSV 23*, 10 – 14 July 2016, Athènes, Greece.

[6] V. Kutis, *Modelling of FGM and piezoelectric beam members using FEM*, Slovak University of Technology Bratislava, 2014.

[7] V. Giurgiutiu, Lamb Wave Generation with Piezoelectric Wafer Active Sensors for Structural Health Monitoring, *8th Annual International Symposium on NDE for Health Monitoring and Diagnostics*, 2–6 March 2002, San Diego, https://doi.org/10.1117/12.483492.

[8] Z. Wu, X-Q. Bao, V. K. Varadan, V.V. Varadan, Light-weight robot using piezoelectric motor, sensor and actuator, *Smart Materials and Structures* 1(4) 1992, pp. 330–340, DOI: 10.1088/0964-1726/1/4/008.

[9] P. Malfi, A. Nicillela, M. Spirto, CH. Cosenza, V. Niola, S. Savino, Motion sensing study on a mobile robot through simulation model and experimental tests, *WSEAS Transactions on Applied and Theoretical Mechanics*, 17, pp. 79–85, 2022, DOI: 10.37394/232011.2022.17.11.

[10] T. R. Chandrupatla, A. D. Belegundu, *Introduction to Finite Elements in Engineering*, 3rd ed., Pearson, New Delhi, 2002.

[11] J. Sladek, P. Novak, P.L. Bishay, V. Sladek, Effective properties of cement-based porous piezoelectric ceramic composites, *Construction and Building Materials*, 190 2018, pp. 1208-1214, DOI: 10.1016/j.conbuildmat.2018.09.127.

[12] M. A. Gokcay, C. Hajiyev, TRIAD-Aided EKF for Satellite Attitude Estimation and Sensor Calibration, *WSEAS Transactions on Applied and Theoretical Mechanics*, 17, pp. 207–214, 2022, https://doi.org/10.37394/232011.2022.17.25.

[13] A. Baksa, I. Ecsedi, Bounding Formulae for the Capacitance of a Cylindrical Two-dimensional Capacitor with Cartesian Orthotropic Dielectric Material, *WSEAS Transactions on Circuits and Systems*, 22 2023, pp. 135-140, https://doi.org/10.37394/23201.2023.22.15.

[14] A.M.A. Al-Kifaie N. N. Hussein, T. N. Jamil, A. A. Akon, A. A. Abojassim, Synthesis and Characterization of Nanoparticle Semiconductor Materials (ZnO) by Hydrothermal Technique, *WSEAS Transactions on Applied and Theoretical Mechanics*, 17, pp. 56–61, 2022, https://doi.org/10.37394/232011.2022.17.8.

[15] Y.A. Utkin, M. Sha, Study of Electrokinetic Properties of Magnetite – Silica Core – Shell Nanoparticles, *WSEAS Transactions on Applied and Theoretical Mechanics*, 16, pp. 172–178, 2021, https://doi.org/10.37394/232011.2021.16.19.

[16] R. G. Geyer, *Dieletric Characterization and Reference materials*, U.S. Government Printing Office, Washington, 1990.

Contribution of Individual Authors to the Creation of a Scientific Article (Ghostwriting Policy)

- Eva Kormanikova carried out the theoretical analysis, conception and writing the paper.
- Kamila Kotrasova carried out the numerical analysis and numerical example by FEM.

Sources of Funding for Research Presented in a Scientific Article or Scientific Article Itself
VEGA1/0363/21, VEGA 1/0307/23

Conflict of Interest
Eva Kormanikova reports financial support was provided by Scientific Grant Agency of the MSVVaS and the SAV.

Alternatively, in case of no conflicts of interest the following text will be published:
The authors have no conflicts of interest to declare.